Check for updates



# Adsorption of phosphorus by alkaline Tunisian soil in a fixed bed column

Rihab Beji, Wissem Hamdi, Aida Kesraoui and Mongi Seffen


## ABSTRACT

The present study evaluates the phosphorus (P) adsorption by alkaline soil in fixed bed column mode operation. The effects of flow rate, bed height, and initial P concentration on breakthrough curves were evaluated. Data confirmed that both the breakthrough and exhaustion time increased in parallel with the rise in bed height and the decline in flow rate and initial P concentration. The adsorption capacity was observed to increase with decreasing flow rate and bed height and increasing initial concentration. Moreover, continuous adsorption experiments were conducted using three salts (NaCl, KCl and $CaCl_2$) with the same concentration (0.01 M) to investigate the P adsorption behavior in saline conditions. The results showed that all three salts improve the P adsorption in the soil column. Consequently, the bed performance was significantly enhanced with salts addition. The maximum adsorption capacity of 13.47 mg $g^{-1}$ for P, 16.13 mg $g^{-1}$ for P-NaCl, 22.10 mg $g^{-1}$ for P-KCl, 30.05 mg $g^{-1}$ for P-$CaCl_2$ was attained at an initial influent concentration of 300 mg $g^{-1}$, bed height of 22 cm, and flow rate of 10 mL $min^{-1}$. The$CaCl_2$ addition was therefore the most effective in increasing P adsorption. Thomas, Yoon-Nelson and Clark models were applied to experimental results to forecast the breakthrough curves by nonlinear regression analysis. Meanwhile, the bed depth service time model was employed to examine the effective model parameters in scaling up the process using linear regression analysis. The values of correlation coefficient ($R^2$) and the sum of squared error evidenced that the Thomas model is the most appropriate model to fit the experimental data. The reusability experiment showed that the adsorbent material still had high P adsorption capacity, and tolerable desorption efficiency.


**Key words** | adsorption, breakthrough curve, modeling, phosphorus, salts, soil

**Rihab Beji**
Faculty of Sciences of Monastir,
Monastir University,
Monastir,
Tunisia

**Rihab Beji**
**Wissem Hamdi**
**Aida Kesraoui** (corresponding author)
**Mongi Seffen**
Laboratory of Energies and Materials (LabEM):
Lr11ES34, Higher School of Science and Technology of Hammam Sousse,
Sousse University,
Sousse,
Tunisia
E-mail: *aida.kesraoui@gmail.com*

**Wissem Hamdi**
Higher Institute of the Sciences and Techniques of Waters of Gabès,
Gabes University,
Gabes,
Tunisia

## NOMENCLATURE

| | |
|---|---|
| $C_0$ | Influent P concentration (mg $L^{-1}$) |
| $C_r$ | Phosphorus removal concentration (mg $L^{-1}$) |
| $C_t$ | Effluent P concentration (mg $L^{-1}$) |
| $K_\alpha$ | Rate constant in bed depth service time (BDST) model (L $mg^{-1}$ $min^{-1}$) |
| $K_{Th}$ | Kinetic rate constant of Thomas model (mL $min^{-1}$ $mg^{-1}$) |
| $K_{YN}$ | Rate constant of Yoon-Nelson model ($min^{-1}$) |
| m | Weight of adsorbent packed within the column (g) |
| n | Freundlich parameter |
| $N_0'$ | Adsorption capacity from BDST model (mg $L^{-1}$) |
| $P_{total}$ | Total amount of P entering the column |
| $q_0$ | Equilibrium P uptake per gram of adsorbent from Thomas model (mg $g^{-1}$) |
| $q_{eq}$ | Weight of P adsorbed per gram of adsorbent from experiment (mg $g^{-1}$) |
| $q_{total}$ | Total weight of P adsorbed by adsorbent in column (mg) |
| Q | Volumetric flow rate (mL $min^{-1}$) |
| r | Clark model constant |
| t | Effluent time (min) |
| $t_{total}$ | Total flow time (min) |
| Y | Removal percentage of P (%) |
| $\tau$ | Time essential for 50% adsorbate breakthrough from Yoon-Nelson model (min) |
| $\tau_{exp}$ | Time essential for 50% adsorbate breakthrough from experiments (min) |

doi: 10.2166/wst.2018.341

Downloaded from http://iwaponline.com/wst/article-pdf/78/4/751/487231/wst078040751.pdf
by guest

## INTRODUCTION

Phosphorus (P) is an essential crop nutrient, extensively used in many industrial and agricultural applications. It is generally present at a low concentration in the environment, being the limiting factor for aquatic plant growth (Rout *et al.* 2014). However, the increasing discharge of P is taking place through human population growth, urbanization, and agricultural and industrial expansion. The enormous inputs of P to aquatic ecosystems has resulted in serious environmental issues such as eutrophication, which affects the quality of domestic, agricultural, and recreational water resources (Huang *et al.* 2013). The drawbacks of eutrophication include harmful algal blooms, ecological and economic losses of impacted waters, loss of oxygen, and fisheries habitat destruction (Yang *et al.* 2008). Therefore, the importance of reducing P inputs in order to control eutrophication, promote fertilization, and save drinking water supplies has been widely recognized (Conley *et al.* 2009).

Recently, numerous studies have investigated ways and means for P removal from aqueous solutions, including chemical precipitation, physical processes, biological treatment and adsorption-based processes. Of the various processes, adsorption is a promising technique that has the benefit of high removal efficiency, easy availability of an extensive range of adsorbents and effective operation (Zhou *et al.* 2015). Soil possesses the potential to be utilized for cost-effective removal of P thanks to its cheapness, easy availability, and great adsorptive capacity (Ioannou *et al.* 2013). In the present study, we focused on evaluating the P adsorption potential and the effect of three salts (NaCl, KCl, $CaCl_2$) used with the same concentration (0.01 M) in a fixed bed column. During previous studies (Hamdi *et al.* 2015), phosphorus adsorption kinetics in soils was investigated via batch tests. The use of soils as potential adsorbents for P removal has been proved. However, batch adsorption is inappropriate for utilization in industry, as huge treatment volumes are continuously generated. It is necessary to evaluate fixed bed adsorption data to obtain more realistic results. Moreover, continuous flow experiments can provide valuable information for increasing the design and operation of phosphorus adsorption processes. As a continuation of the previous batch studies (Hamdi *et al.* 2015), the present investigation concerns the performance evaluation of soils for P removal in column mode of operation. The effects of parameters such as bed height, flow rate and initial P concentration on breakthrough curves were examined. The fixed-bed adsorption data were validated by various dynamic models such as Thomas model, Yoon-Nelson model, and Clark model using non linear regression analysis. Error analysis was carried out to examine the adequacy and accuracy of the model equations. A regeneration experiment was undertaken to check the adsorbent reusability.

## MATERIALS AND METHODS

### Adsorbent

The P adsorption investigation was carried out using soil samples of the semi-arid areas of Chott Meriem (40° 3′ N 9°10′ E), Tunisia. The soil was washed with distilled water to eliminate surface-adhered particles and dried at 100 °C. Subsequently, the adsorbent was ground and sieved and particle sizes of 2 mm were used as adsorbent in the adsorption study. The adsorbent physicochemical properties are shown in Table 1. Powder X-ray diffraction (XRD) patterns were used to determine the quantitative mineralogical analysis.

**Table 1** | Physicochemical properties of sampled soils (Hamdi *et al.* 2015)

| Properties and composition | Value |
|---|---|
| pH | 8.12 |
| Particle size | <2 mm |
| Organic matter (%) | 1.5 |
| P (ppm) | 90 |
| Cation exchange capactity (meq per 100 g soil) | 19.72 |
| $C_{org}$ (mg $kg^{-1}$) | 10,980 |
| Ca (mg $kg^{-1}$) | 5,450 |
| Al (mg $kg^{-1}$) | 76 |
| K (mg $kg^{-1}$) | 491 |
| Na (mg $kg^{-1}$) | 57.50 |
| Mn (mg $kg^{-1}$) | 9.15 |
| Fe (mg $kg^{-1}$) | 33.57 |
| Zn (mg $kg^{-1}$) | 3.64 |
| Cu (mg $kg^{-1}$) | 2.74 |
| Mg (mg $kg^{-1}$) | 410.10 |
| Cd (mg $kg^{-1}$) | 0.05 |
| Clay % | 12.80 |
| Sand % | 49.20 |
| Silt % | 15.40 |

Downloaded from http://iwaponline.com/wst/article-pdf/78/4/751/487231/wst078040751.pdf
by guest

## Adsorbate

The P stock solution of 1,000 mg $L^{-1}$ was obtained using dihydrogen phosphate ($KH_2PO_4$) powders (analytical reagent grade, Panreac 99%). This solution was diluted using distilled water in order to prepare experimental working solutions with various concentrations. A synthetic P solution of 300 mg $L^{-1}$ was utilized for optimizing operating parameters in continuous adsorption studies. The P-NaCl, P-KCl and P-$CaCl_2$ solutions were prepared by adding 0.01 M of NaCl, KCl, and $CaCl_2$ (Sigma-Aldrich 98–100.5%) to the prepared P solution.

## Chemical and physical analysis

Soil analysis was performed on the air-dried and sieved samples. The pH of this adsorbent was accessed using distilled water in a 1:2 (mass) soil:solution ratio. The pipette method allows the determination of particle size distribution. The specific surface area was obtained by a porosimeter accelerated surface area and porosimetry system (model ASAP 2010). The Walkley–Blac procedure (Hamdi *et al.* 2015) allows the determination of the organic carbon ($C_{org}$). The solution was titrated against ammonium ferrous sulfate [$Fe(NH_4)_2(SO_4)_2.6H_2O$], using diphenylamine indicator. The concentrations of P, Ca, Mg, K, Fe, Na, Al, Cd, Cu and Mn were obtained using Mehlich-III methods (Mehlich 1984) by equilibrating 2.5 g of air-dried soil with the extracting solution of Mehlich-III (25 mL) for 5 min and percolating through Whatman No. 40 filter paper. An inductively coupled plasma optical emission spectrophotometer (Perkins Elmer, Model 4300DV) was used to determine the concentrations of the different elements of the extract. Powder XRD data were recovered to establish the mineralogical analysis using an internal standard for each mineral. The clay fraction was quantified after purification and based on a pure standard clay mineral. Panalytical CubixX' Pert Pro diffractometer, with $CuK_\lambda$ radiation, $\lambda =$ 1.5418 Å in the 2Θ angle range of 2°–40° was adopted to obtain the powder XRD patterns (Hamdi *et al.* 2015).

## FTIR studies

Surface functional groups of the adsorbent were analyzed using Fourier transform infrared spectrometry (FTIR, Perkin Elmer Spectrum Two) for the 4,000–400 $cm^{-1}$ spectrum range. The transmission spectrum was achieved with 4 $cm^{-1}$ resolution and corrected for a KBr background. Infrared spectra of pure and P-adsorbed adsorbent were recorded.

## Fixed bed column studies

Fixed bed column adsorption experiments were executed using a copper column of 1.5 cm inner diameter and 50 cm height. At the top and bottom of the column, a porous sheet was placed followed by a glass wool to prevent loss of the material and avoid outlet clogging. The column was filled with the adsorbent, and distilled water was infiltrated through the bed. Adsorption experiments were achieved in the down flow mode through the fixed bed column using a peristaltic pump (easy-Load 07516–00). Effluent solutions were gathered until exhaustion. Operating parameters including the initial concentration of P solutions (100, 300 and 500 mg $L^{-1}$), bed height (13, 22 and 31 cm), and flow rate (8, 10 and 12 mL $min^{-1}$) were varied. The residual P concentration was determined using a spectrophotometer (Biochrome Libra S22) at maximum wavelength 868 nm.

## Mathematical description

The data acquired from column studies were used to obtain the breakthrough curves by plotting $C_t/C_0$ (the ratio of effluent and influent phosphate concentration) vs. time (t). For a desired initial concentration and flow rate, the quantity of total P adsorbed in the fixed bed column ($q_{total}$) can be accessed from the area under the breakthrough curve using the following formula:

$$q_{total} = \frac{Q}{1000} \int_{t=0}^{t=t_{total}} C_r \, dt \quad (1)$$

where Q is the volumetric flow rate (mL $min^{-1}$) and $C_r = C_0 - C_t$ is the P removal concentration (mg $L^{-1}$).

The equilibrium phosphate adsorption capacity of the column, $q_{eq}$ (mg $g^{-1}$), is obtained as follows:

$$q_{eq} = \frac{q_{total}}{m} \quad (2)$$

where m is the weight of adsorbent packed within the column (g).

The total amount of P entering the column ($P_{total}$) can be acquired using the equation given below:

$$P_{total} = \frac{C_0 \; Qt_{total}}{1000} \quad (3)$$

where $t_{total}$ is the exhaustion time (min).

Downloaded from http://iwaponline.com/wst/article-pdf/78/4/751/487231/wst078040751.pdf
by guest

The removal percentage of P (Y) can be acquired as the following:

$$Y(\%) = \frac{q_{total}}{P_{total}} \times 100 \quad (4)$$

The effluent P concentration remaining in residual solution can be calculated using the following equation:

$$C_t = \frac{P_{tot} - q_{total}}{V_{eff}} \quad (5)$$

where $V_{eff}$ is the effluent volume (mL) that can be calculated as $V_{eff} = Q \times t_{total}$

The mass transfer zone (MTZ), is the region of the bed where most of the adsorption occurs and moves up the bed with time and can be calculated from:

$$MTZ = L\frac{t_e - t_b}{t_e} \quad (6)$$

where L is the bed height (cm), $t_b$ is the time required to reach the breakthrough point (min), and $t_e$ is the time required to reach the exhaust point (min).

The time of contact between the water phase and the adsorbent is termed as empty bed contact time (EBCT). EBCT (min) basically measures the critical depth and the contact time for an adsorbent. It can be calculated as per the following equation:

$$EBCT = \frac{V}{Q} \quad (7)$$

where V = adsorbent bed volume (mL).

## Modeling of column adsorption data

The prediction of the concentration–time profile from the breakthrough curves provides successful design of a continuous adsorption process. In order to examine the dynamic performance of P adsorption onto soil of Chott Meriem region, several models were introduced to fit the column experimental data, namely bed depth service time (BDST), Thomas, Clark and Yoon-Nelson.

### Thomas model

The Thomas equation is applied to evaluate the performance theory of the adsorption process in a fixed-bed column. The model supposes that reversible reactions follow the second-order kinetics and the Langmuir isotherm. This model can be well used notably in the absence of internal and external diffusion resistances (Azzaz *et al.* 2017).

The form of the Thomas model is depicted using the following equation:

$$\frac{C_t}{C_0} = \frac{1}{1 + \exp\left[K_{Th}\left(\frac{q_0 m}{Q} - C_0 t\right)\right]} \quad (8)$$

where $C_t$ is the effluent P concentration at time t (mg $L^{-1}$), $C_0$ is the influent P concentration (mg $L^{-1}$), Q is the flow rate (mL $min^{-1}$), m is the weight of adsorbent in the column (g), t is the time (min), $K_{Th}$ is the kinetic rate constant for the Thomas equation (mL $mg^{-1}$ $min^{-1}$), and $q_0$ is the equilibrium P uptake per gram of adsorbent from Thomas equation (mg $g^{-1}$).

### Clark model

Clark (1987) used the mass-transfer concept jointly with the Freundlich isotherm in favor of describing a new simulation of breakthrough curves as:

$$\frac{C_t}{C_0} = \left(\frac{1}{1 + Ae^{-rt}}\right)^{\frac{1}{n-1}} \quad (9)$$

From a plot of $C_t/C_0$ against t at a given flow rate and bed height using nonlinear regressive analysis, the Clark model parameter A and the rate of mass transfer r were obtained.

### Yoon-Nelson model

Yoon-Nelson is applied to predict the saturation time and the performance of removal process for a known adsorbate concentration. This model supposes that the rate of decline in the probability of adsorption for each adsorbate molecule is directly proportional to the probability of the adsorbate molecule adsorption and the adsorbate breakthrough on the adsorbent. The Yoon-Nelson model is less complicated than other models and necessitates no detailed data regarding the physicochemical properties of adsorbate and adsorbent (Gong *et al.* 2015). The mathematical expression of the model is expressed as:

$$\frac{C_t}{C_0} = \frac{\exp(K_{YN}t) - \tau K_{YN}}{1 + (\exp(K_{YN}t) - \tau K_{YN})} \quad (10)$$

Downloaded from http://iwaponline.com/wst/article-pdf/78/4/751/487231/wst078040751.pdf
by guest

where $K_{YN}$ is the rate constant of Yoon-Nelson model ($min^{-1}$), and $\tau$ (min) is the time essential for 50% breakthrough point.

The approach involves a plot of $C_t/C_0$ vs. sampling time (t) according to Equation (10). The values of $K_{YN}$ and $\tau$ can be obtained using the nonlinear regressive method.

### BDST model

The BDST model is assigned to the physical measurement of bed capacity at various values of percentage breakthrough. The BDST model constants provide the process enlargement for other flow rates and concentrations without further experimentations. It is applied to predict the dynamic performance of any bed length, if data for some depths are recognized. It supposes that the bed depth, Z, and service time, t, of a column show a linear relationship. The model supposes that the rate of adsorption is under control of the surface reaction between the adsorbate and the unused capacity of the adsorbent (Dissanayake *et al.* 2016).

The BDST equation can be made explicit as follows:

$$t = \frac{N'_0}{C_0 F} Z - \frac{1}{K_\alpha C_0} \ln\left(\frac{C_0}{C_t} - 1\right) \quad (11)$$

where $C_0$ is the influent P concentration (mg $L^{-1}$), $C_t$ is the effluent P concentration at time t (mg $L^{-1}$), $N'_0$ is the bed adsorption capacity (mg $L^{-1}$), F is the linear velocity (cm $min^{-1}$), t is the effluent time (min), Z is the column bed depth (cm), and $K_\alpha$ is the rate constant in the BDST model (L $mg^{-1}$ $min^{-1}$).

A plot of t versus Z should exhibit a linear relationship where $N'_0$ and $k_\alpha$ can be obtained from the slope and intercept of the plot, respectively.

Linear and nonlinear regression analyses were performed in order to determine the fixed-bed model parameters for the experimental and predicted data of $C_t/C_0$ for each model. Sum of squared error (SSE; Equation (12)) and $R^2$ values were adopted in order to validate the most applicable model that would describe the adsorption performance of the breakthrough curves in the fixed-bed column.

$$SSE = \frac{\sum [(C_t/C_0)_c - (C_t/C_0)_e]^2}{N} \quad (12)$$

where $(C_t/C_0)_c$ is the ratio of effluent and influent P concentrations acquired from the model calculation, $(C_t/C_0)_e$ is the ratio of effluent and influent P concentrations acquired from the experiment and N is the number of experimental points.

## RESULTS AND DISCUSSION

### Characterization of the adsorbent

The physicochemical composition of the soil of Chott Meriem region is illustrated in Table 1. The pH value was 8.12 revealing that the soil is alkaline. The basic nature of the studied adsorbent is associated with the great concentration of some basic cations, specifically calcium and magnesium, from the different horizons of the soils (Hamdi *et al.* 2015). It was reported in our previous work (Beji *et al.* 2017) that phosphate ions can react with Fe and Al-oxides by ligand exchange forming inner-sphere complexes whereas the presence of Ca ions facilitates P removal via precipitation. The soil was rich in exchangeable calcium representing 5,450 mg $kg^{-1}$. The mechanism of P immobilization by calcium may be the formation of calcium phosphate precipitation by the reaction of dissolved $Ca^{2+}$ with the phosphate in the solution (Hamdi *et al.* 2015). Moreover, mineral analysis in Table 2 indicates that the texture was dominated by the sand.

### FTIR studies

Figure 1 presents the FTIR spectrum of soil sample of Chott Meriem. The infrared spectra present a large number of peaks, which prove the complex nature of the studied adsorbent. The absorption band at 3,430.15 $cm^{-1}$ is assigned to OH groups' stretching vibration (Franco *et al.* 2017). The band appearing at 1,632.61 $cm^{-1}$ corresponds to HOH

**Table 2** | Soil mineralogical composition (Hamdi *et al.* 2015)

| | Kaolinite | Quartz | Calcite | Smectite | Illite | chlorite |
|---|---|---|---|---|---|---|
| Abundance of mineralogy | + | +++ | + | + | − | − |

+++ abundant, + poorly abundant.

Downloaded from http://iwaponline.com/wst/article-pdf/78/4/751/487231/wst078040751.pdf
by guest

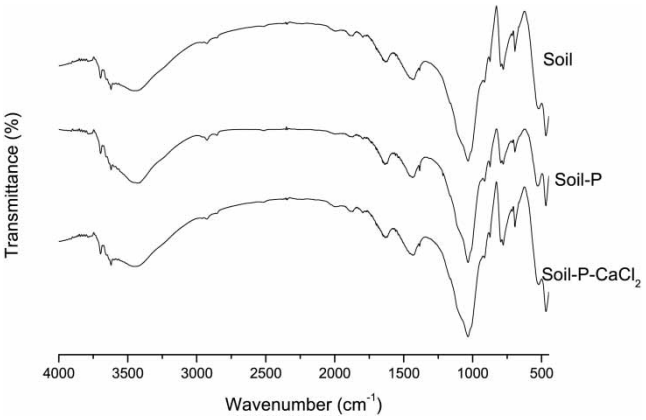


**Figure 1** | Spectra of soil, soil-P, and soil-P-$CaCl_2$.

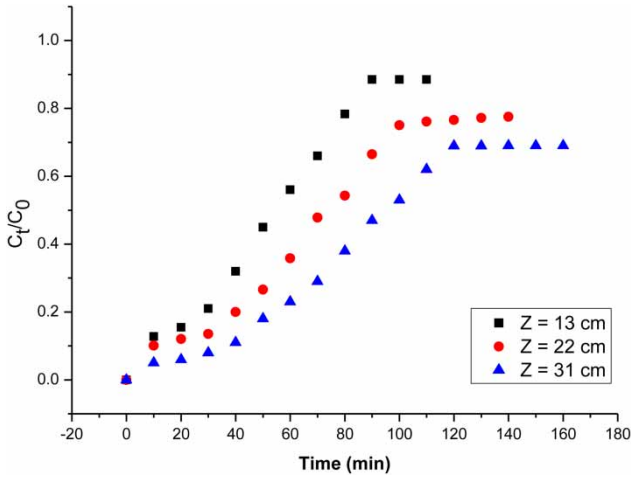


**Figure 2** | Breakthrough curves: the effect of different bed depths on P adsorption ($C_0 = 300$ mg $L^{-1}$, $Q = 10$ mL $min^{-1}$).

deformation of adsorbed water (Saikia & Parthasarathy 2010). The peak at 1,432.89 $cm^{-1}$ is ascribed to carbonate stretching vibration (Li *et al.* 2015). The band located at 1,033.46 $cm^{-1}$ is attributed to P=O stretching vibration (Alimohammadi *et al.* 2016). The band at 778.72 $cm^{-1}$ is assigned to Si-O stretching of quartz (Saikia & Parthasarathy 2010). In addition, the peak present at 532.25 $cm^{-1}$ is associated with P-O bending (Wang *et al.* 2010). The peak at 469.92 $cm^{-1}$ corresponds to Si-O-Si deformation (Saikia & Parthasarathy 2010). Reaction with P and P-$CaCl_2$ caused a shift in these absorption bands. The strengthening intensity of the peaks related to P-O and P=O bending after adsorption indicates the P addition (from 35.31% to 37.31% and from 14.23% to 19.81%, respectively) (Beji *et al.* 2017). The addition of P-$CaCl_2$ also causes a rise in the intensity of these bands (from 35.31% to 48.4% in the case of P-O bending and from 14.23% to 30.99% in the case of P=O stretching), which confirms P adsorption. These results are in agreement with the findings reported in our earlier work (Beji *et al.* 2017). On the other hand, the two latter absorption bands were present even before P exposure, indicating the presence of these functionalities in the adsorbent surface.

## Fixed bed column studies

### Effect of bed height

In order to examine the impact of bed height on the fixed bed removal of P, bed heights were varied as 13, 22 and 31 cm with a constant flow rate of 10 mL $min^{-1}$ and initial P concentration of 300 mg $L^{-1}$. The related breakthrough curves are introduced in Figure 2. It is clear from the figure that with increasing bed heights (from 13 to 22 to 31 cm), breakthrough and exhaustion times were extended. This result could be explained by the longer bed height providing further EBCT between the adsorbent and the adsorbate (Table 3). In addition, the breakthrough curve slopes declined with rising bed heights, leading to a broadened mass transfer zone. The increase in P removal efficiency with the increase of bed height (Table 3) could be attributed to a greater amount of soil present in the fixed bed, which implies that there are more binding sites available for P adsorption (Zhou *et al.* 2015).

### Effect of different flow rates

The breakthrough curves at different flow rates of 8, 10 and 12 mL $min^{-1}$ are introduced in Figure 3. The results-showed that when the flow rate rose from 8 to 12 mL $min^{-1}$, the breakthrough and exhaustion times were reduced notably. This could be attributed to the increase of rate of mass transfer with flow rate increasing. As evidenced in Table 3, with a rise of flow rate, the percentage removal and adsorption capacity declined from 62.32 to 38.86% and from 14.02 to 10.24 mg $g^{-1}$, respectively. The EBCT decreased with the increase of flow rate (Table 3). Therefore, the lower flow rate provided greater adsorbate–adsorbent interaction and diffusion of P within the adsorbent, exploiting the biggest portion of the adsorbent bed (Rout *et al.* 2014). As a result, exhaustion time increased, which promotes better column performance (Xu *et al.* 2014). Similar outcomes were recorded by Banerjee *et al.* (2017) when investigating Cr(VI) removal by shells in a fixed bed column system.

Downloaded from http://iwaponline.com/wst/article-pdf/78/4/751/487231/wst078040751.pdf
by guest

**Table 3** | Adsorption breakthrough data for different bed heights, flow rates, and initial P concentrations

| $C_0$ (mg $L^{-1}$) | Q (mL $min^{-1}$) | Z (cm) | Y (%) | $q_{eq}$ (mg $g^{-1}$) | $C_t$ (mg $L^{-1}$) | MTZ (cm) | EBCT (min) |
|---|---|---|---|---|---|---|---|
| 100 | 10 | 22 | 66.80 | 5.01 | 33.20 | 21.23 | 3.8 |
| 300 | 10 | 22 | 55.26 | 13.47 | 134.10 | 21.10 | 3.8 |
| 500 | 10 | 22 | 50.77 | 14.27 | 257.00 | 21.11 | 3.8 |
| 300 | 8 | 22 | 62.32 | 14.02 | 113.10 | 21.29 | 4.8 |
| 300 | 12 | 22 | 38.86 | 10.24 | 183.60 | 21.07 | 3.2 |
| 300 | 10 | 13 | 52.91 | 14.28 | 141.30 | 12.10 | 2.2 |
| 300 | 10 | 31 | 59.90 | 10.36 | 120.30 | 30.28 | 5.4 |

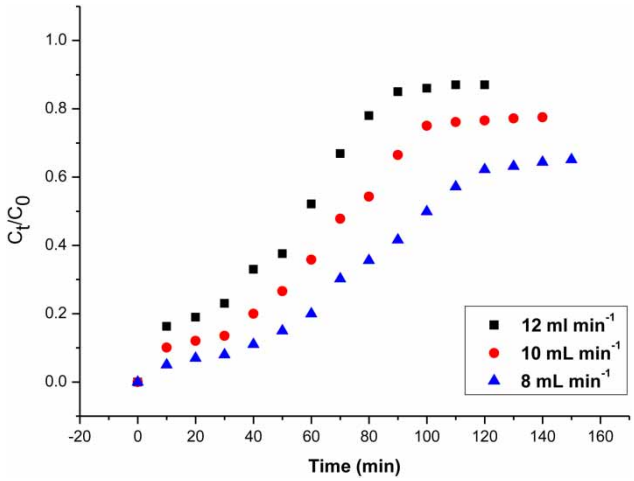


**Figure 3** | Breakthrough curves: the effect of flow rate on P adsorption ($C_0 = 300$ mg $L^{-1}$, Z = 22 cm).

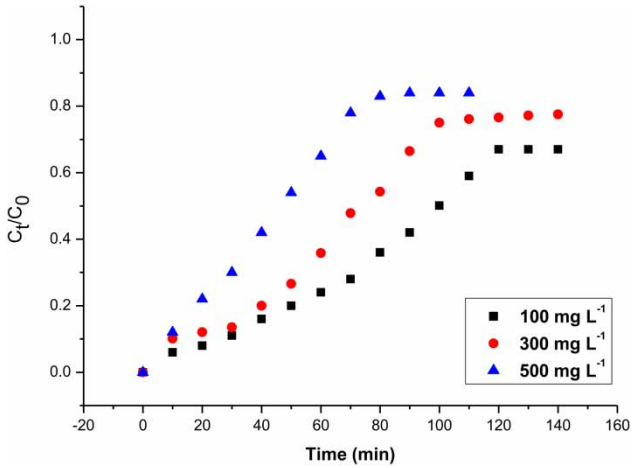


**Figure 4** | Breakthrough curves: the effect of influent concentration on P adsorption (Q = 10 mL $min^{-1}$, Z = 22 cm).

## Effect of influent P concentration

The breakthrough curves under varying influent P concentration as 100, 300 and 500 mg $L^{-1}$ are presented in Figure 4. It is evident from the figure that both breakthrough and saturation time declined with increasing influent P concentration. At higher influent concentration, the breakthrough curves were sharper and breakthrough occurred quicker as compared to the case of lower influent concentration where flatter breakthrough curves and slower bed exhaustion were obtained. This can be illustrated by the fact that higher adsorbent sites were being occupied with the rise of P concentration. These results prove that the change of concentration gradient influences the breakthrough time as well as the saturation rate (Han *et al.* 2009). In addition, an increase in P uptake capacity (from 5.01 to 14.27 mg $g^{-1}$) can be observed for an increasing of initial P concentration from 100 to 300 mg $L^{-1}$.

## Effect of salts on the bed performance

New experiments were performed with P, P-NaCl, P-KCl and P-$CaCl_2$ solutions (0.01 M of all salts) to explore the effect of salts on the bed performance at the same experimental conditions. The results are introduced in Figure 5 and Table 4. It is evident that the three salts added to the P solution provide improvements on the breakthrough curves. The most considerable enhancement was noticed when P-$CaCl_2$ was used. In this case, breakthrough time reaching saturation increased, the maximum adsorption capacity grew from 13.47 to 30.05 mg $g^{-1}$ and the removal percentage rose by 28% (compared with the P control sample) (Table 4). The results emphasize that all three salts could increase the P adsorption in the soil column compared with the control sample. This can be explained on the basis that addition of salts increases the soil ionic strength. Thus, P adsorption tended to increase (Curtin *et al.* 1993). On the other hand, at greater values of pH,

Downloaded from http://iwaponline.com/wst/article-pdf/78/4/751/487231/wst078040751.pdf
by guest

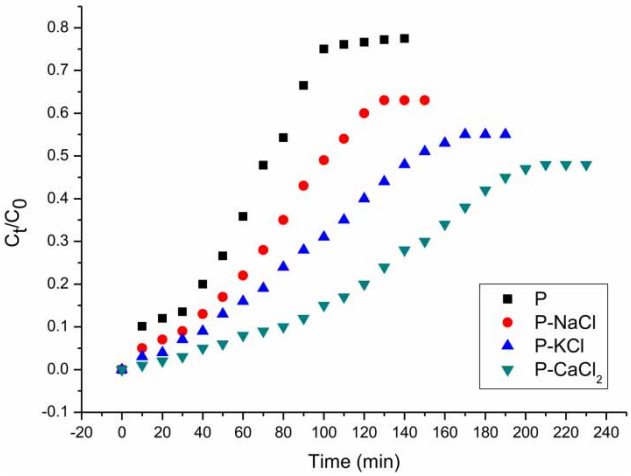


**Figure 5** | Breakthrough curves: the effect of three salts on P adsorption ($C_0 = 300$ mg $L^{-1}$, $Q = 10$ mL $min^{-1}$, $Z = 22$ cm).

**Table 4** | Parameters of the dynamic models in the fixed bed adsorption of P, P-NaCl, P-KCl, P-$CaCl_2$ by the alkaline soil

| | Adsorbate | | | |
|---|---|---|---|---|
| **Models** | **P** | **P-NaCl** | **P-KCl** | **P-$CaCl_2$** |
| Thomas | | | | |
| $K_{Th}$ ($\times 10^4$), L $mg^{-1}$ $min^{-1}$ | 1.1 | 0.8 | 0.6 | 0.5 |
| $q_e$, mg $g^{-1}$ | 14.49 | 20.53 | 29.05 | 39.94 |
| $R^2$ | 0.966 | 0.965 | 0.953 | 0.967 |
| SSE ($\times 10^3$) | 3.02 | 2.01 | 1.91 | 0.68 |
| Y, % | 51.31 | 66.17 | 69.3 | 80.13 |
| $q_{e(exp)}$, mg $g^{-1}$ | 1 3.47 | 16.13 | 22.10 | 30.05 |
| Clark | | | | |
| A | 22.88 | 10.93 | 5.75 | 14.97 |
| r ($\times 10^2$), $min^{-1}$ | 3.6 | 2.3 | 1.46 | 1.38 |
| $R^2$ | 0.962 | 0.968 | 0.962 | 0.971 |
| SSE ($\times 10^3$) | 3.47 | 1.84 | 1.54 | 0.91 |
| Yoon-Nelson | | | | |
| $K_{YN}$ ($\times 10^3$), L $min^{-1}$ | 2.61 | 1.44 | 2.06 | 1.08 |
| $\tau$, min | 377.82 | 488.36 | 698.39 | 949.94 |
| $R^2$ | 0.942 | 0.974 | 0.981 | 0.973 |
| SSE ($\times 10^3$) | 5.22 | 1.47 | 0.75 | 0.78 |
| $\tau_{exp}$, min | 66.16 | 75.46 | 90.99 | 130 |

salts can neutralize the negatively charged phosphate molecule and the negatively charged surface of soil, facilitating the latter to adsorb more phosphate molecules (Ip *et al.* 2009).

Considering $q_{eq}$ and Y values, it can be concluded that all salts were favorable for the continuous adsorption of P. Due to salt addition, the bed performance was increased as exhibited in Figure 5 and Table 4.

Table 4 shows that the salt addition generally improves the adsorption of P on the soil; moreover, this is carried out in a descending order: P-$CaCl_2$ > P-KCl > P-NaCl > P. These results can be attributed respectively to the low, medium, and high solubility of Ca-phosphates, K-phosphates, and Na-phosphates (Beji *et al.* 2017). Furthermore, this arrangement of salts to enhance P removal can be linked with the valence degree and hydration of cations brought with chloride ($Ca^{2+}$, $K^+$, $Na^+$). One possible reason is that divalent cations can fit into cavities of adsorbed phosphate ions (Beji *et al.* 2017). This behavior favors the adsorption of P ions on $Ca^{2+}$ cations. In addition, potassium and sodium are two monovalent cations with different hydrated radii (3.31 and 3.58 Å respectively). Sodium is more hydrated than potassium such that water molecules are more bound in the inner sphere hydration shell in the $Na^+$ case. Dykstar *et al.* (2016) found that potassium ions are preferentially adsorbed over sodium considering their greater mobility.

It was verified in Table 4 that $CaCl_2$ exhibited the best performance to be applied in fixed bed adsorption of P. In this work, using a column with a height of 50 cm and a diameter of 1.5 cm, flow rate of 10 mL $min^{-1}$, and influent P concentration of 300 mg $L^{-1}$, the maximum adsorption capacity value was 30.05 mg $g^{-1}$ (Table 4). Rout *et al.* (2014) evaluated the adsorption of phosphate by a mixture of ground burnt patties and red soil in a fixed bed column. They used a column with a diameter of 4.5 cm and studied the effect of initial concentration (5 and 15 mg $L^{-1}$), flow rate (2.5, 5 and 7.5 mL $min^{-1}$) and bed height (10, 15 and 20 cm). Under these conditions, the $q_{eq}$ values ranged from 0.858 to 2.112 mg $g^{-1}$. This result demonstrates that the soil studied in presence of $CaCl_2$ can be an option for fixed bed adsorption of P.

To establish the relative efficiency of Chott Meriem soils relative to others used to remove phosphorous from aqueous solutions, a comparison was made on the basis of the maximum adsorption capacity ($q_{eq}$). The comparison (Table 5) revealed that soils of Chott Meriem region could be considered as a promising material to remove phosphorus when compared to volcanic ash soil (Nguyen & Maeda 2016), ground burnt patties and red soil (Rout *et al.* 2014), zirconium loaded okara (Nguyen *et al.* 2015), and slag filter media (Lee *et al.* 2014). The higher adsorption capacity reveals that our adsorbent had a better potential of adsorption relative to other adsorbent materials.

Downloaded from http://iwaponline.com/wst/article-pdf/78/4/751/487231/wst078040751.pdf
by guest

**Table 5** | Comparison of adsorption capacities between Chott Meriem soils and other studied adsorbents

| Adsorbents | Adsorption capacity (mg $g^{-1}$) | References |
|---|---|---|
| Volcanic ash soil | 5.57 | Nguyen & Maeda (2016) |
| Ground burnt patties and red soil | 2.11 | Rout *et al.* (2014) |
| Zirconium loaded okara | 12.21 | Nguyen *et al.* (2015) |
| Slag filter media | 0.018 | Lee *et al.* (2014) |
| Chott Meriem soils | 16.56 | This study |

## Breakthrough curve modeling

### Analysis using the Thomas model

The column data were fitted to the Thomas model to determine the Thomas rate constant ($K_{Th}$) and maximum solid-phase concentration ($q_0$) using nonlinear regression analysis. The Thomas model parameters and the values of $R^2$ and SSE at different experimental conditions are introduced in Tables 4 and 6.

It is clear from Table 6 that as the influent concentration increased, $q_0$ values decreased while $K_{Th}$ values increased. This is related to the driving force difference for adsorption that follows the concentration gradient. When the flow rate increased, $q_0$ values increased while $K_{Th}$ values decreased. Thus, lower flow rate and higher influent concentration provided better adsorption efficiency. Additionally, it was found that $q_0$ values, predicted using the Thomas model, are close to the $q_{eq}$ values accessed from experimental data for given experimental conditions. As indicated in the data (Table 4), $K_{Th}$ values varied with chemical modification and the following classification was exhibited: P > P-NaCl > P-KCl > P-$CaCl_2$. On the other hand, it is clear that $q_{eq}$ values were enhanced with salts addition and the following classification was exhibited: P-$CaCl_2$ > P-KCl > P-NaCl > P.

The elevated $R^2$ values (0.952 to 0.991) and low SSE values (0.00068 to 0.00317) (Tables 4 and 6) revealed the suitableness of fit between the experimental results and corresponding predicted values using the Thomas model.

### Analysis using the Clark model

The Freundlich constant values ($n = 2.24$ (P); $n = 1.87$ (P-NaCl); $n = 1.68$ (P-KCl); $n = 1.83$ (P-$CaCl_2$)) obtained from the batch experiments in our previous work were used to calculate the parameters in the Clark model. The values of A and r in the Clark model were obtained from Equation (9) using nonlinear regression analysis and are introduced in Tables 4 and 7.

From Table 7, as both flow rate and influent P concentration increased, the rate of mass transfer (r) increased. However, with the bed height increase, r values decreased. Also, it is clear from Table 4 that A and r values declined with the addition of the following salts: NaCl, KCl and $CaCl_2$. The elevated values of $R^2$ (0.947–0.99) and low values of SSE (0.00091–0.00366) advocated that the Clark model presented a convenient correlation on the effects of evaluated parameters.

### Analysis using the Yoon-Nelson model

A simple theoretical model as presented in Equation (10) was applied to evaluate the breakthrough performance of P removal in column mode. $K_{YN}$ and $\tau$ values are listed in Tables 4 and 8.

**Table 6** | Parameters of Thomas model using nonlinear regression analysis and the equilibrium P uptake ($q_{eq}$) and total removal percentage (Y) for P adsorption at various bed-heights, flow rates, and initial P concentrations

| $C_0$, mg $L^{-1}$ | Q, mL $min^{-1}$ | Z, cm | $K_{Th}$ ($\times 10^4$), mL $min^{-1}$ $mg^{-1}$ | $q_0$, mg $g^{-1}$ | $R^2$ | SSE ($\times 10^3$) |
|---|---|---|---|---|---|---|
| 100 | 10 | 22 | 2.8 | 6.35 | 0.983 | 0.99 |
| 300 | 10 | 22 | 1.1 | 14.49 | 0.966 | 3.02 |
| 500 | 10 | 22 | 0.9 | 15.09 | 0.970 | 3.17 |
| 300 | 8 | 22 | 0.9 | 16.15 | 0.964 | 2.26 |
| 300 | 12 | 22 | 1.5 | 12.77 | 0.981 | 2.06 |
| 300 | 10 | 13 | 1.7 | 16.56 | 0.991 | 0.99 |
| 300 | 10 | 31 | 1.0 | 11.60 | 0.952 | 2.44 |

Downloaded from http://iwaponline.com/wst/article-pdf/78/4/751/487231/wst078040751.pdf
by guest

**Table 7** | Parameters of the Clark model using nonlinear regression analysis at various bed heights, flow rates, and initial P concentrations

| $C_0$, mg $L^{-1}$ | Q, mL $min^{-1}$ | Z, cm | A | r ($\times 10^2$), $min^{-1}$ | $R^2$ | SSE ($\times 10^3$) |
|---|---|---|---|---|---|---|
| 100 | 10 | 22 | 32.15 | 3.08 | 0.980 | 1.17 |
| 300 | 10 | 22 | 22.88 | 3.6 | 0.962 | 3.47 |
| 500 | 10 | 22 | 15.92 | 5.01 | 0.965 | 3.66 |
| 300 | 12 | 22 | 30.85 | 2.87 | 0.945 | 2.63 |
| 300 | 8 | 22 | 21.42 | 4.79 | 0.979 | 2.20 |
| 300 | 10 | 13 | 27.56 | 5.37 | 0.990 | 1.12 |
| 300 | 10 | 31 | 31.17 | 3.14 | 0.962 | 2.87 |

As shown in Table 8, the bed height increase leads to the increase of $\tau$ values and the decrease of $K_{YN}$ values. On the other hand, $K_{YN}$ values increased whereas $\tau$ values declined with rising flow rate and influent P concentration. The increase of $K_{YN}$ value was due to the increased driving force of mass transfer in the liquid film (Liu *et al.* 2017), which explains the result that the breakthrough and saturation occurred faster at higher flow rate and initial concentration. These findings are similar to those obtained by earlier researchers in fixed-bed adsorption studies (Tsai *et al.* 2016). Also, the data (Table 4) indicated that $K_{YN}$ values were reduced with the addition of salts and the following decreasing arrangement was determined: P > P-NaCl > P-KCl > P-$CaCl_2$. It is observed in Table 8 that $\tau$ values obtained from the model were much higher than those obtained from experiments under all experimental conditions, revealing that the Yoon-Nelson model is unsuitable in predicting the $\tau$ values due to its relative simplicity. The high values of nonlinear regression coefficient (0.913–0.981) and low values of error (0.00075–0.00926) indicated the accuracy of the Yoon-Nelson equation to fit the obtained experimental data using nonlinear regression.

## Analysis using the BDST model

The BDST plots for P removal at 20, 40 and 60% breakthroughs for a flow rate of 10 mL $min^{-1}$ and initial phosphate concentration of 300 mg $L^{-1}$ are shown in Figure 6. The adsorption capacity ($N_0'$) and rate constant were accessed from the slope and intercept of the obtained plots. Table 9 exhibits that there was a consistent rise in the slopes from the breakthroughs of 20–60% and a subsequent enhancement in the corresponding values of adsorption capacity (from 1,841 to 4,059 mg $L^{-1}$). This result can be explained by the fact that at a lower breakthrough value, some active sites of the adsorbent were still not covered by phosphate anions; thus, it remained unsaturated. The fixed bed adsorption capacity at such a low breakthrough position was therefore lower than the total column adsorption capacity of the material. It is evident that $R^2$ values were above 0.99 indicating the adequacy of the BDST model to describe the present continuous system. Additionally, the obtained BDST model constants can be useful to scale-up the process for other flow rates and concentrations without further experimentation runs.

## Comparison of Thomas, Yoon-Nelson and Clark models

The statistical parameters R2 and SSE were employed to determine the best mathematical model out of Thomas, Yoon-Nelson and Clark models. As listed in Tables 4 and 6–8, the range of $R^2$ values from the Thomas model (0.952–0.991) were the highest, followed by the Clark and Yoon-Nelson model with respective values of 0.945–0.99 and 0.913–0.981 at the same operating conditions. Similarly, SSE values from the Thomas model (0.00068–0.00317) were lower than that of Clark (0.00091–0.00366) and Yoon-Nelson (0.00075–0.00926) models. Thus, it was concluded that the Thomas model was the most appropriate to describe the process of P adsorption rather than the Clark and

**Table 8** | Yoon-Nelson parameters using nonlinear regression analysis at various bed heights, flow rates, and initial P concentrations

| $C_0$, mg $L^{-1}$ | Q, mL $min^{-1}$ | Z, cm | $K_{YN}$ ($\times 10^3$), L $min^{-1}$ | $\tau$, min | $R^2$ | SSE ($\times 10^3$) | $\tau_{exp}$, min |
|---|---|---|---|---|---|---|---|
| 100 | 10 | 22 | 2.26 | 447.40 | 0.981 | 1.16 | 83.10 |
| 300 | 10 | 22 | 2.61 | 377.82 | 0.942 | 5.22 | 66.10 |
| 500 | 10 | 22 | 3.37 | 280.88 | 0.913 | 9.26 | 40.00 |
| 300 | 10 | 22 | 2.13 | 474.25 | 0.968 | 1.98 | 78.71 |
| 300 | 8 | 22 | 3.22 | 299.58 | 0.942 | 6.32 | 53.65 |
| 300 | 12 | 13 | 3.62 | 271.68 | 0.966 | 3.95 | 51.89 |
| 300 | 10 | 31 | 2.29 | 442.83 | 0.964 | 2.72 | 77.63 |

Downloaded from http://iwaponline.com/wst/article-pdf/78/4/751/487231/wst078040751.pdf
by guest

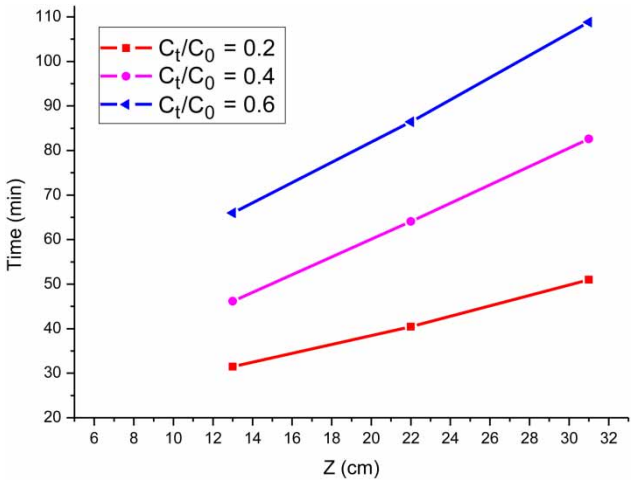


**Figure 6** | BDST model for different bed heights ($C_0 = 300$ mg $L^{-1}$, $Q = 10$ mL $min^{-1}$), $C_t/C_0 = 0.2$, 0.4, 0.6 correspond to 20%, 40%, 60% breakthrough values.

**Table 9** | Calculated constants of the BDST model for the adsorption of P ($C_0 = 300$ mg $L^{-1}$, $Q = 10$ mL $min^{-1}$)

| $C_t/C_0$ | a, min $cm^{-1}$ | b, min | $K_\alpha \times 10^4$, L $mg^{-1}$ $min^{-1}$ | $N_0'$, mg $L^{-1}$ | $R^2$ |
|---|---|---|---|---|---|
| 0.2 | 1.08±13.1 | 17.1±0.04 | 2.70 | 1,841.68 | 0.996 |
| 0.4 | 2.02±0.5 | 19.77±0.02 | 0.68 | 3,449.74 | 0.999 |
| 0.6 | 2.38±1.4 | 34.71±0.06 | −0.38 | 4,059.03 | 0.998 |

Yoon-Nelson models. The elevated $R^2$ values and low SSE values demonstrated that all applied models are useful to predict the fixed bed column adsorption process following the order as: Thomas > Clark > Yoon-Nelson.

### P adsorption/desorption and reusability

The fixed bed column was subjected to a desorption process after saturation to regenerate the material for consecutive reuse. In this study, desorption experiments were executed by passing distilled water through the saturated bed at a flow rate of 10 mL $min^{-1}$. Figure 7 presents the results of adsorption/desorption cycles. The P adsorption capacity in the first cycle was 13.47 mg $g^{-1}$ and it gradually declined to 10.82 mg $g^{-1}$ after three cycles, which is almost 80.5% of the original adsorption capacity. The capacity loss by extending the number of adsorption/desorption cycles is associated with the occupancy of some adsorbent active sites by the non-desorbed P and the destruction of the layered structure of the material. On the other hand, desorption capacity was maintained well above 90% of the original capacity in the third cycle, proving the reusability of the adsorbent.

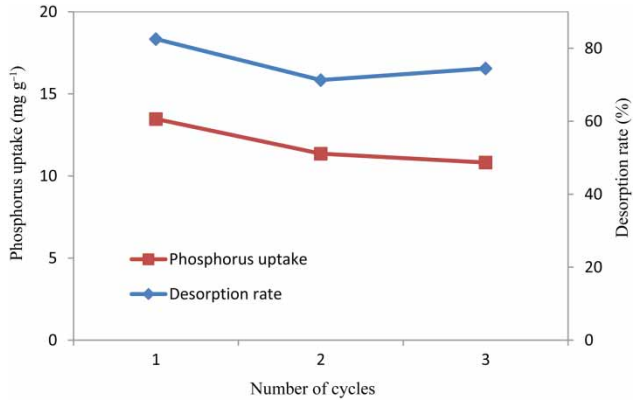


**Figure 7** | Phosphorus uptake and reusability in cycle assays ($C_0 = 300$ mg $L^{-1}$, 10 mg $L^{-1}$, Z = 22 cm).

## CONCLUSION

The soil sampled from the Chott Meriem region was found to be a favorable cost-effective adsorbent for P adsorption in column mode. The experimental data revealed that the fixed bed adsorption of P was dependent on the flow rate, initial P concentration, bed height and type of dissolved salt. The increase in bed height affected the column performance by delaying the exhaustion time. However, the increase in flow rate and initial P concentration tended to speed up the exhaustion of the column. The total removal percentage of P was increased with the increase of bed height and decrease in flow rate and initial P concentration. Moreover, results revealed that all three types of salt addition were favorable to increase the bed performance in the P adsorption. The BDST model with a perfect linear plot (>0.99), adequately predicts the breakthrough curves. It was found that the Thomas, Yoon-Nelson and Clark models fitted well the continuous adsorption data. The best fitting of the models to the experimental data followed the order: Thomas > Clark > Yoon-Nelson. Exploring the adsorption/desorption capacity of the material demonstrated that the capacity did not notably decline after three consecutive adsorption/desorption cycles. These results support the use of this material for P removal from aqueous solution in continuous systems and show that these soils can retain P and adapt well to fertilization.

## ACKNOWLEDGEMENTS

The authors thank the laboratory of Energy and Materials and the project FP7 FP4BATIW for the funding support.

Downloaded from http://iwaponline.com/wst/article-pdf/78/4/751/487231/wst078040751.pdf
by guest

## REFERENCES


Alimohammadi, Z., Younesi, H. & Bahramifar, N. 2016 Batch and column adsorption of reactive red 198 from textile industry effluent by microporous activated carbon developed from walnut shells. *Waste Biomass Valor.* **8**, 1255–1270. doi: 10.1007/s12649-016-9506-4.

Azzaz, A. A., Jelleli, S., Souissi, R., Ergaieg, K. & Bousselmi, L. 2017 Alkaline-treated sawdust as an effective material for cationic dye removal from textile effluents under dynamic conditions: breakthrough curve prediction and mechanism exploration. *Environ. Sci. Pollut. Res.* **24** (22), 18240–18256. doi: 10.1007/s11356-017-9388-4.

Banerjee, M., Bar, N., Basu, R. K. & Das, S. K. 2017 Comparative study of adsorptive removal of Cr(VI) ion from aqueous solution in fixed bed column by peanut shell and almond shell using empirical models and ANN. *Environ. Sci. Pollut. Res.* **24** (11), 10604–10620. https://doi.org/10.1007/s11356-017-8582-8.

Beji, R., Hamdi, W., Kesraoui, A. & Seffen, M. 2017 Effects of salts on phosphorus adsorption in alkalize Tunisian soil. *Euro-Mediterr. J. Environ. Integ.* **2** (2), 1–9. doi: 10.1007/s41207-016-0012-7.

Clark, R. M. 1987 Evaluating the cost and performance of field-scale granular activated carbon systems. *Environ. Sci. Technol.* **21** (6), 573–580. doi: 10.1021/es00160a008.

Conley, D. J., Paerl, H. W., Howarth, R. W., Boesch, D. F., Seitzinger, S. P., Havens, K. E., Lancelot, C. & Likens, G. E. 2009 Controlling eutrophication: nitrogen and phosphorus. *Ecology* **323**, 1014–1015. doi: 10.1126/science.1167755.

Curtin, D., Steppuhn, H. & Selles, F. 1993 Plant responses to sulfate and chloride salinity: growth and ionic relations. *Soil Sci. Soc. Am. J.* **57** (5), 1304–1310. doi: 10.2136/sssaj1993.03615995005700050024x.

Dissanayake, D. M. R. E. A., Chathuranga, P. K. D., Perera, P. I., Vithanage, M. & Iqbal, M. C. M. 2016 Modeling of Pb(II) adsorption by a fixed-bed column. *Bioremediat. J.* **20** (3), 194–208. http://dx.doi.org/10.1080/10889868.2016.1212808

Dykstar, J. E., Dijkstra, J., Wal, A., Hamelers, H. V. M. & Porada, S. 2016 On-line method to study dynamics of ion adsorption from mixtures of salts in capacitive deionization. *Desalination* **390**, 47–52. https://doi.org/10.1016/j.desal.2016.04.001.

Franco, D. S. P., Tanabe, E. H. & Dotto, G. L. 2017 Continuous adsorption of a cationic dye on surface modified rice husk: statistical optimization and dynamic models. *Chem. Eng. Commun.* **204** (6), 625–634. http://dx.doi.org/10.1080/00986445.2017.1300150.

Gong, J. L., Zhang, Y. L., Jiang, Y., Zeng, G. M., Cui, Z. H., Liu, K., Deng, C. H., Niu, Q. Y., Deng, J. H. & Huan, S. Y. 2015 Continuous adsorption of Pb(II) and Methylene Blue by engineered graphite oxide coated sand in fixed-bed column. *App. Surf. Sci.* **330**, 148–157. http://dx.doi.org/10.1016/j.apsusc.2014.11.068.

Hamdi, W., Noura, Z., Ernest, K., Didier, B., Frederic, G. & Mongi, S. 2015 Effect of the soils properties on the sorption capacity of phosphorus and ammonium by alkaline soils of the semi-arid areas. *IOSR-J. A. C* **8** (5), 34–42. doi: 10.9790/5736-08513442.

Han, R., Wang, Y., Zhao, X., Wang, Y., Xie, F., Cheng, J. & Tang, M. 2009 Adsorption of methylene blue by phoenix tree leaf powder in a fixed-bed column experiments and prediction of breakthrough curves. *Desalination* **245** (1), 281–297. https://doi.org/10.1016/j.desal.2008.07.013.

Huang, W., Li, D., Zhu, Y., Xu, K., Li, J., Han, B. & Zhang, Y. 2013 Phosphate adsorption on aluminum-coordinated functionalized macroporous silica: surface structure and adsorption behavior. *Mater. Res. Bull.* **48** (12), 4974–4978. https://doi.org/10.1016/j.materresbull.2013.04.093.

Ioannou, Z., Dimirkou, A. & Ioannou, A. 2013 Phosphate adsorption from aqueous solutions onto goethite, bentonite, and bentonite-goethite system. *Water Air Soil Pollut.* **224**, 1374–1382.

Ip, A., Baford, J. P. & McKay, G. 2009 Reactive black dye adsorption/desorption onto different adsorbents: effect of salt, surface chemistry, pore size and surface area. *J. Colloid Interface Sci.* **337** (1), 32–38. doi: 10.1016/j.jcis.2009.05.015.

Lee, C. G., Kim, G. H., Kang, G. K., Kim, S. B., Park, S. G., Lee, S. H. & Choi, J. W. 2014 Comparative analysis of fixed bed adsorption models using phosphate breakthrough curves in slag filter media. *Desalination Water Treat.* **55** (7), 1–11. https://doi.org/10.1080/19443994.2014.930698.

Li, Y., Cai, J., Song, G. & Ji, J. 2015 DRIFT spectroscopic study of diagenetic organic–clay interactions in argillaceous source rocks. *Spectrochim. Acta A, Mol. Biomol. Spectrosc.* **148**, 138–145. doi: 10.1016/j.saa.2015.03.131.

Liu, J., Xia, S., Lü, X. & Shen, H. 2017 Adsorption of tricresyl phosphate onto grapheme nanomaterials from aqueous solution. *Water Sci. Technol.* **76**, 1565–1573. doi: 10.2166/wst.2017.317.

Mehlich, A. 1984 Mehlich3 soil test extractant: a modification of Mehlich 2 extractant. *Commun. Soil Sci. Plant Anal.* **15** (12), 1409–1416.

Nguyen, H. V. & Maeda, M. 2016 Removal of phosphorus from water by using volcanic ash soil (VAS): batch and column experiments. *Water Sci. Technol.* **77** (11), 1–9. doi: 10.2166/wst.2016.297.

Nguyen, T. A. H., Ngo, H. H., Guo, W. S., Mham, T. Q., Li, F. M., Nguyen, T. V. & Bui, X. T. 2015 Adsorption of phosphate from aqueous solutions and sewage using zirconium loaded okara (ZLO): fixed-bed column study. *Sci. Total. Environ.* **523**, 40–49. https://doi.org/10.1016/j.scitotenv.2015.03.126.

Rout, R. P., Dash, R. R. & Bhunia, P. 2014 Modelling and packed bed column studies on adsorptive removal of phosphate from aqueous solutions by a mixture of ground burnt patties and red soil. *Adv. Environ. Res.* **3** (3), 231–225. http://dx.doi.org/10.12989/aer.2014.3.3.231.

Saikia, B. J. & Parthasarathy, G. 2010 Fourier transform infrared spectroscopic characterization of kaolinite from Assam and Meghalaya, Northeastern India. *J. Mod. Phys.* **1** (4), 206–210. doi:10.4236/jmp.2010.14031.

Tsai, W. C., Luna, M. D. G., Arriesgado, H. L., Futalan, C. M., Colades, J. I. & Wan, M. W. 2016 Competitive fixed-bed


Downloaded from http://iwaponline.com/wst/article-pdf/78/4/751/487231/wst078040751.pdf
by guest

adsorption of Pb(II), Cu(II), and Ni(II) from aqueous solution using chitosan-coated bentonite. *Int. J. Polym. Sci.* **2016** (2016), 1–11.

Wang, Y. P., Law, R. M. & Pak, B. 2010 A global model of carbon, nitrogen and phosphorus cycles for the terrestrial biosphere. *Biogeosciences* **7**, 2261–2282. doi: 10.5194/bg-7-2261-2010.

Xu, X., Gao, B., Tan, X., Zhang, X., Yue, Q., Wang, Y. & Li, Q. 2014 Adsorption of Congo red from solution using cationic surfactant modified wheat straw in column model B. *Chem. Eng. J.* **2** (1), 40–45. https://doi.org/10.1016/j.jece.2013.11.025.

Yang, X., Wu, X., Hao, H. & He, Z. 2008 Mechanisms and assessment of water eutrophication. *J. Zhejiang Univ. Sci. B* **9** (3), 197–209. doi: 10.1631/jzus.B0710626.

Zhou, T., Lu, W., Liu, L., Zhu, H., Jiao, Y., Zhang, S. & Han, R. 2015 Effective adsorption of light green anionic dye from solution by CPB modified peanut in column mode. *J. Mol. Liq.* **211**, 909–914. https://doi.org/10.1016/j.molliq.2015.08.018.

First received 3 February 2018; accepted in revised form 21 July 2018. Available online 31 July 2018

Downloaded from http://iwaponline.com/wst/article-pdf/78/4/751/487231/wst078040751.pdf
by guest